DOI: 10.24352/UB.OVGU-2019-009 TECHNISCHE MECHANIK, 39, 1, (2019), 85 – 96
submitted: July 6, 2018

Modelling of Heat Transfer and Fluid Flow through a Granular Material and External Wall Barrier

E. Szymanek, A. Tyliszczak

Heat and fluid flow simulations for granular material in wall barriers allow to design them in a way that maximally reduces the expenditures on utilisation of buildings. This paper demonstrates the solution to the problem of the passage of air through the external wall barrier. It shows how the temperature changes inside the wall barriers when the external temperature changes. Two types of partitions are tested: single-layer (granular material) and two-layer (granular and concrete material). The paper presents comparison of the results of the numerical model and in-house code with the experimental data. The numerical model applied is based on the unsteady equation of heat conduction (3D) and the Navier-Stokes equations. A high-order compact method in combination with the WENO scheme and predictor-corrector method are applied for the spatio-temporal discretisation. The flows of air and heat in the granular layers are modelled using immersed boundary technique, which allows to use Cartesian meshes for objects with very complex geometric shapes. The correctness of numerical model applied has been verified by comparisons with ANSYS Fluent results and experimental data obtained from measurements performed in a laboratory and in-situ.

1 Introduction

The process of heat transfer occurs wherever temperature differences exists and a material has conductive properties. It is very common and present in many technological branches. This paper is devoted to an analysis of the heat and fluid flow through granular materials, which are important to a vast array of industries. For instance, in chemical engineering and catalytic reactors, where large surfaces of packed granular beds intensify chemical reactions (Alvarez de Miguel et al., 2014; Yancy-Caballero et al., 2018), in energy production systems, where granulates are promising materials for heat storage and heat transfer media (Baumann and Zunft, 2014; Ma et al., 2014; Ratuszny, 2017), in spray drying and spray granulation installations (Hoffmann et al., 2015; Diez et al., 2018) or in construction industry, where the granular layers are used for wall barrier and heat insulators (Szymanek et al., 2014). In this last example the knowledge of temperature distribution is necessary both to evaluate the efficiency of materials used for wall barrier as well as to assess the correctness of their construction method. In this type of applications the granular materials are currently regarded as one of the most demanding systems. Description of the heat transfer in granulates in the same way as in solids, liquids or gases is impossible and requires the analysis of a number of interrelated processes and the use of increasingly advanced computational and experimental methods. Difficulty is caused by the fact that empty spaces between the granular particles can be filled with gas or water (see Fig. 1) and the heat exchange can take place between them as well as with the granular material, thus leading to a coupled complex problem. Certainly, precise explanations of the phenomena occurring between the constituents in granular systems could be helpful for designing not only new type of wall barriers with improved control of temperature changes but also for all aforementioned industrial branches.

Measurements of the flow behaviour in complex granular structures are often based on sophisticated imaging techniques (Hainswoeth and Aylmore, 1983) including tomographic methods based on X-rays (Computed Tomography, CT) (Breugen et al., 2014). Attempts of theoretical descriptions of the transport processes inside the granular layers are not fully successful and require knowledge of many empirical parameters. Some of the models describing the heat transfer through the granular bed are based on formulas for homegenous medium assuming that over the time the differences between the phases disappear and fluid and solid materials have similar temperatures (Amhalhel and Furmaski, 1997).

In line with rapid development of computational technology the granular layers are more and more studied using numerical methods. Various modelling approaches have been developed for these purposes, they all belong to the

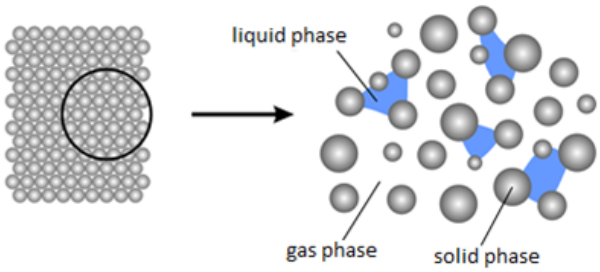

Figure 1: Three-phase granular bed system

CFD (Computational Fluid Dynamics) methods and are based on continuous models (Massoudi, 2006) including finite element/finite volume methods (FEM/FVM), lattice Boltzmann techniques (LBM) or fractional calculus (Szymanek et al., 2014). Vargas and McCarthy (Vargas and McCarthy, 2001) have developed a TPD (thermal particle dynamics) method based on the Discrete Element Method (DEM) allowing analysis of grain-grain interactions. This approach was also used to describe the heat and mass flow in granular beds by Ferrez and Liebling (Ferrez and Liebling, 2001). In their work the granular beds were treated as systems consisting of solid bodies and a system of different pore sizes filled with liquid, gas or a mixture of them. A similar approach to the problem was presented in (Tian and Shu, 2009), where the granular material was described as a homogeneous bed consisting of elements of irregular structure (porous, granular). Ordonez and Alvarado (Ordonez and Alvarado, 2010) proposed a model of heat transfer through a granular bed taking into account the temperature of the solid and gaseous phase separately.

Despite the above mentioned advanced studies the complexity of the flow and thermal processes occurring inside the layer causes that in many cases researchers focus an analyses of simplified problems taking account granular particles with simple shapes. For instance, isolated spheres were studied by Fornberg B. (Fornberg, 1988), while interactions between two spheres being in close proximity were analysed by Dixon et al. (Dixon et al., 2011). Recently, Li et al. (Li et al., 2017), investigated the flows and heat transfer around two spheres using the large eddy simulation (LES) method. An analysis of interactions occurring in this flow type cane can be also found in (Qi et al., 2018), where the flow between two interactive particles was studied using a three-dimensional lattice Boltzmann model.

In the present paper we concentrate on numerical studies of the heat and mass flow in granular layers composed of spherical objects located in a stream of flowing medium or in a wall barrier. The numerical model applied in this paper allows to precisely compute the inner temperature distributions and their variability over time. The solver used in this research is an in-house code called SAILOR. It is based on the unsteady equation of heat conduction (3D) and the Navier-Stokes equations, which allow modeling the airflow in the cases in which the walls are made of permeable granular materials. The analysed problem is treated as unsteady and the flow is assumed to be laminar. The solution algorithm is based on the projection method for determining the pressure field and velocity. A high-order compact method in combination with the WENO scheme and predictor-corrector method are applied for the spatio-temporal discretisation. The flows of air and heat in the granular layers are modelled using immersed boundary (IB) technique, which allows the use of Cartesian meshes for objects with very complex geometric shapes. It was demonstrated that the IB method can be used for modelling of laminar and turbulent flow regimes with domains changing in time and moving objects and with heat exchange (Fadlun et al., 2000, Mittal and Iaccarino, 2005). Concerning discretisation methods it has been successfully applied along with the spectral methods and finite/compact difference methods. In this work we apply probably the simplest variant of the IB method, i.e., the so-called *volume penalisation* method (IB-VP), also known as *fictitious domain* (Mittal and Iaccarino, 2005, Khadra et al., 2000) method. In the IB-VP approach the fluid is penalized from entering a solid part of a domain by adding a continuous forcing term to the equations governing the heat and fluid flow. The forcing extends throughout the entire volume of solid body and is not just confined to a neighbourhood of the solid interface. What makes the IB-VP method very attractive is the simple implementation and the use of an easily definable phase-indicator function (mask function), which by ”switching-on / off” easily identifies the computational nodes as fluid or solid parts. The correctness of applied numerical model has been verified by ANSYS Fluent and by experimental data obtained from measurements performed in a laboratory and using real bulkheads. The purpose of the experiment was to determine the internal temperature distributions and their variability in respect to a changing temperature outside the bulkheads. During the measurements the samples were placed in a climate chamber that could be accurately controlled. It enabled to simulate real outdoor conditions and on the basis of the obtained results, temperature profiles in layers were created.

2 Mathematical Modelling

In this paper we consider variable temperature and variable density flows. The changes of density are caused by increasing/decreasing wall temperature and they are larger than acceptable by Boussinesq approximation. We consider therefore a low Mach number flow described by the continuity equation, the Navier-Stokes equations and the energy equation, which in the framework of an IB-VP approach are defined as:

$$\partial_t \rho + \nabla \cdot (\rho \mathbf{u}) = 0 \tag{1}$$

$$\rho \left(\partial_t \mathbf{u} + (\mathbf{u} \cdot \nabla)\mathbf{u}\right) + \nabla p \mathbf{I} = \nabla \cdot \boldsymbol{\tau} + \mathbf{f}^{\mathrm{IB}} \tag{2}$$

$$\rho C_p \left(\partial_t T + (\mathbf{u} \cdot \nabla) T\right) = \nabla \cdot (\kappa \nabla T) + \mathrm{f}_T^{\mathrm{IB}} \tag{3}$$

The set of Eqs. (1)-(3) is complemented with the equation of state $p_0 = \rho R T$. In open flows with inlet/outlet boundaries p_0 is constant in space and time (Tyliszczak, 2016). The molecular viscosity (μ) within $\boldsymbol{\tau}$ is computed from the Sutherland law. The source terms $\mathbf{f}^{\mathrm{IB}}$ and $\mathrm{f}_T^{\mathrm{IB}}$ originate from the IB method and their role is to act on a fluid in such a way as if there were a solid object immersed in the flow domain.

2.1 Solution Algorithm

The solution algorithm for Eqs. (1-3) is formulated in the framework of a projection method (Fletcher, 1991) for pressure-velocity coupling with a direct forcing approach for the IB method (Mittal and Iaccarino, 2005). The time integration is based on a predictor-corrector approach (Adams-Bashforth/Adams Moulton) and the spatial discretisation is performed using 6th/5th order compact difference and WENO (Weighted Essentially Non-Oscilatory) schemes on half-staggered meshes (Tyliszczak, 2014, Tyliszczak, 2016). In the framework of the IB approach the solution algorithm is defined as follows.

Predictor step. Generally, we assume that the time-step (Δt) can vary as the flow velocity changes in the successive time-steps, $..., n-1, n, n+1, ...$ With this assumption the 2nd order Adams-Bashforth method is given as:

$$\begin{aligned} \frac{\rho \boldsymbol{u}^* - \rho \mathbf{u}^n}{\Delta t^n} = &\left(1 + \frac{\Delta t^n}{2\Delta t^{n-1}}\right) \mathrm{Res}(\mathbf{u}^n) \\ &- \frac{\Delta t^n}{2\Delta^{n-1}} \mathrm{Res}(\mathbf{u}^{n-1}) - \nabla p^n \mathbf{I} + \mathbf{f}^{\mathrm{IB}} \end{aligned} \tag{4}$$

$$\begin{aligned} \frac{T_i^* - T_i^n}{\Delta t^n} = &\left(1 + \frac{\Delta t^n}{2\Delta t^{n-1}}\right) \mathrm{Res}(T^n) \\ &- \frac{\Delta t^n}{2\Delta^{n-1}} \mathrm{Res}(T^{n-1}) + \frac{1}{\rho C_p} \mathrm{f}_T^{\mathrm{IB}} \end{aligned} \tag{5}$$

where $\mathrm{Res}(\boldsymbol{u})$, $\mathrm{Res}(T)$ represents the convection and diffusion terms of the Navier-Stokes and energy equations. The formulas for the source terms $\mathbf{f}^{IB}$ and f_T^{IB} are discussed latter. The velocity field $\boldsymbol{u}^*$ computed from Eq. (4) does not fulfil the continuity equation (i.e. $\partial_t \rho + \nabla \cdot (\rho \boldsymbol{u}^*) \neq 0$) and according to the projection method (see (Fletcher, 1991)) it must be corrected using the gradients of pressure correction (p') according to the following formula:

$$\rho \boldsymbol{u}^{**} = \rho \boldsymbol{u}^* - \Delta t^n \nabla p' \boldsymbol{I} \tag{6}$$

where p' is computed from the Poisson equation:

$$\nabla \cdot (\nabla p' \boldsymbol{I}) = \frac{1}{\Delta t^n} \left[\nabla \cdot (\rho \boldsymbol{u}^*) + \partial_t \rho^*\right] \tag{7}$$

resulting from the condition $\partial_t \rho + \nabla \cdot (\rho \boldsymbol{u}^{**}) = 0$. The density is computed from the equation of state $p_0 = \rho^* R T^*$ and its time derivative needed in (7) is disrcretized using 2nd order formula

$$\begin{aligned} \partial_t \rho^* = \frac{(\Delta t^n \Delta t^{n-1})^{-1}}{(\Delta t^n + \Delta t^{n-1})} \Big\{ &\left[(\Delta t^n + \Delta t^{n-1})^2 - (\Delta t^n)^2\right] \bar{\rho}^* \\ &-(\Delta t^n + \Delta t^{n-1})^2 \bar{\rho}^n + (\Delta t^n)^2 \bar{\rho}^{n-1} \Big\} \end{aligned} \tag{8}$$

Corrector step. The 2nd order Adams-Moulton method is defined as:

$$\frac{\rho\mathbf{u}^* - \rho\mathbf{u}^n}{\Delta t^n} = \frac{1}{2}(\text{Res}(\mathbf{u}^{**}) + \text{Res}(\mathbf{u}^n)) - \nabla p^n \mathbf{I} + \mathbf{f}^{\text{IB}} \tag{9}$$

$$\frac{T^{n+1} - T^n}{\Delta t^n} = \frac{1}{2}(\text{Res}(T^{**}) + \text{Res}(T^n)) + \frac{1}{\rho C_p}\text{f}_T^{\text{IB}} \tag{10}$$

Again, the velocity field $\mathbf{u}^*$ does not fulfil the continuity equation and its correction is defined as:

$$\rho\mathbf{u}^{n+1} = \rho\mathbf{u}^* - \Delta t^n \nabla p' \mathbf{I} \tag{11}$$

The equation $\rho_t + \nabla \cdot (\rho\mathbf{u}^{n+1}) = 0$ leads to the Poisson equation (7). Its solution allows us to correct the velocity using (11) and to update the pressure field as:

$$p^{n+1} = p^n + p' \tag{12}$$

The density is computed from $p_0 = \rho^* R T^{n+1}$ and the next time step begins.

IB-VP source term. The IB-VP method works through penalizing a difference between the actual and assumed velocity and temperature of the solid body. The role of the source terms $\mathbf{f}^{\text{IB}}$ and f_T^{IB} is to mimmic the presence of solid objects in the flow domain. In the volume penalization variant of the IB method they are defined as:

$$\mathbf{f}^{\text{IB}} = -\frac{\rho}{\eta}\Gamma(\mathbf{x})(\mathbf{u} - \mathbf{u}_s), \quad \text{f}_T^{\text{IB}} = -\frac{\rho C_p}{\eta}\Gamma(\mathbf{x})(T - T_s) \tag{13}$$

where $\eta \ll 1$ is the so-called penalization parameter with dimension of time unit and Γ - the phase indicator defined as:

$$\Gamma(\mathbf{x}) = \begin{cases} 0, & \text{for } \mathbf{x} \in \Omega_f \\ 1, & \text{for } \mathbf{x} \in \Omega_s \end{cases} \tag{14}$$

For $\Gamma(\mathbf{x}) = 1$ with $\eta \ll 1$ Eqs. 4 and 6 reduce to $\mathbf{u}^* \approx \Delta t^n \mathbf{u}_s/(\eta + \Delta t^n)$ and $T^* \approx \Delta t^n T_s/(\eta + \Delta t^n)$ which for $\eta \ll \Delta t^n$ leads to $\mathbf{u}^* \approx \mathbf{u}_s$ and $T^* \approx T_s$. Thus, the forcing terms enforces the no-slip boundary conditions and set the required temperature of the solid objects. Simplicity of the IB-VP method has, however, direct consequences in lower accuracy. Similarly, as in the classical IB method with a stepwise approach (i.e. without the interpolation (Fadlun et al., 2000)) the formal order of the IB-VP method is at most equal to one (Khadra et al., 2000, Kadoch et al., 2012).

3 Experiment/Laboratory Tests

The correctness of the proposed model has been verified by means of data obtained from experimental research. Two configurations of barriers ($120mm$) were analyzed: granular layer ($120mmm$) and granular ($60mm$)/ concrete ($60mm$) layer. The materials used in construction were concrete and granular material (expanded clay) show at Fig. 2b,c.

Temperature measurements were carried out using the thermocouples placed in holes drilled in layers. The empty spaces between the test center and the thermocouple were filled with drilling dust or pieces of expanded clay, so that the thermocouple would closely adhere to the material being tested. The walls constructed in this way were placed in a climatic chamber Series 3 LTCL600 (TASLtd., WestSussex, UK) (see Fig. 2a), which allowed setting the outside temperature and its precise control during the entire experiment. The thermocouples were placed in layers in many spatial locations. The aim of the experiment was to determine the internal temperature distributions for the changing temperature outside the barriers.

4 Results

4.1 Assessment of the IB-VP Accuracy

As it was mentioned in the previous section the accuracy of the IB-VP method is at most of the first order. Here, we verify how this limitation translates on the results obtained for the cases including the heat and mass transfer

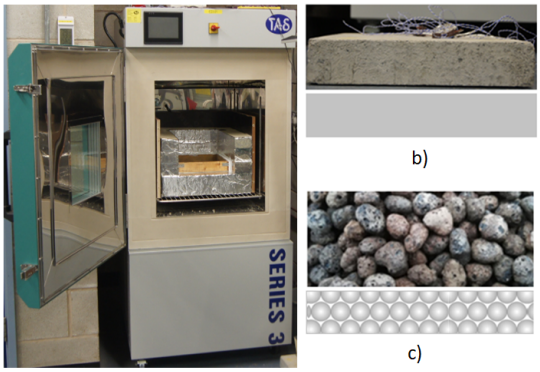

Figure 2: Climatic chamber (a) and material used to wall barrier construction: concrete (b), granular material (c)

in the flows in channels and between or around spheres. The test cases include: (i) an isothermal flow in a channel filled with six layers of spheres, (ii) a flow around heated spheres, (iii) a flow through a bed of granular material and a two-layer bed (granular material with concrete).

In the test case (i), flow through channel filled with a cubic lattice of spheres is examined. The considered configuration consists of six layers of spheres with diameters $D = 28mm$. Their quarters are located in the corners of the channel. The simulations were performed for Reynolds numbers $Re = UD/\nu = 204.74$ (U - inlet velocity, ν - viscosity) $Re = 105.57$, $Re = 59.78$ $Re = 28.88$. The numerical results were compared with experimental data (Suekane et al., 2003) and with the results obtained using the ANSYS Fluent. An important factor affecting the accuracy of the analysis is the density of the mesh. For the SAILOR code the used meshes were regular and uniform and consisted of 40 x 160 x 40 to 80 x 320 x 80 nodes. The simulations performed with ANSYS Fluent were obtained on body-fitted tetrahedral meshes with approximately $2.5 \cdot 10^6$ (mesh M1) and $7 \cdot 10^6$ (M2) tetrahedral cells.

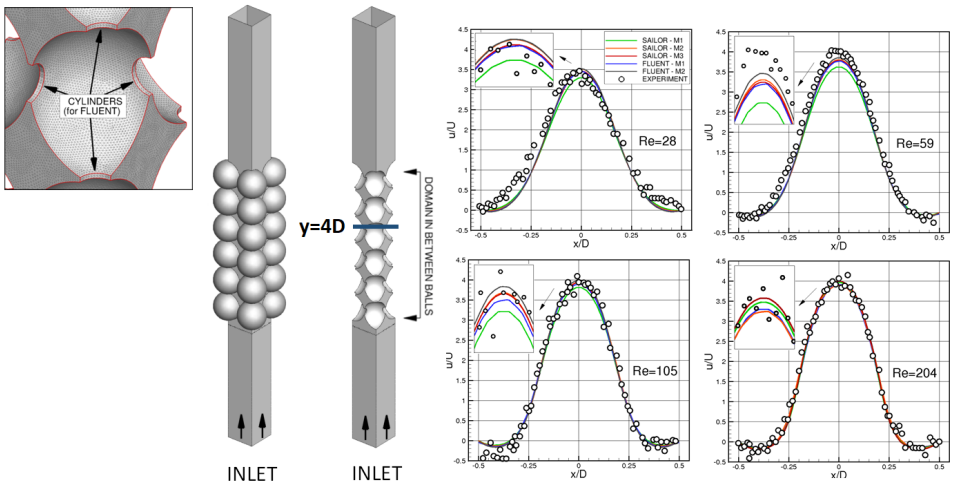

Figure 3: Axial velocity profiles at the location y=4D in a channel filled with six layers of spheres

It can be seen that the results obtained from SAILOR and Fluent practically overlap and are almost independent of the density of the grid. Equally important is that the experimental data are matched very well, see Fig. 3. It can be seen that for the higher the Reynolds number, the convergence of results is better. At $Re = 204$ the computed solutions are in excellent agreement with the experiment. Examination of the profiles at $Re = 28$ reveals a slight discrepancy between the experimental data and numerical results, however, the differences are not large.

In the test case (ii) the flow around three hot spheres ($D = 10mm$) is analysed. The spheres (Fig. 4) have the following coordinates respectively: $(X, Y, Z) = (0.0, 0.0, 0.1)$, $(X, Y, Z) = (-0.0225, 0.0, 0.145)$, $(X, Y, Z) = (0.0225, 0.0, 0.145)$. Temperature of the first sphere is $350K$, while two next have temperature $373K$. The temperature of the incoming flow is $300K$. The flow rate is assigned such that the Reynolds number based on the inlet velocity and sphere diameter is equal to 100.

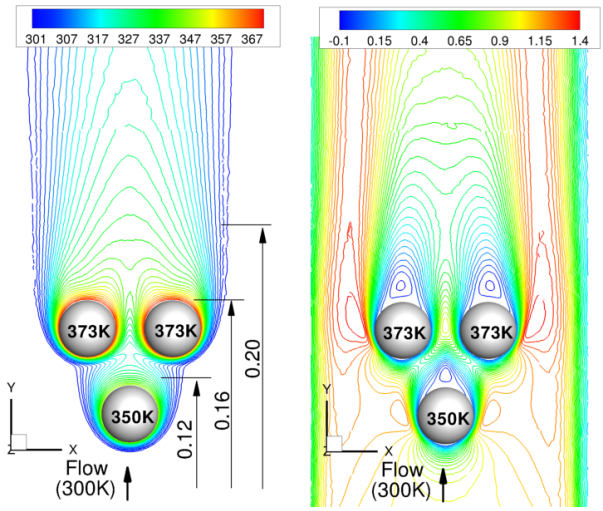

Figure 4: Flow around heated spheres

In this case the grids contained respectively $121 \times 160 \times 121$ (M1) and $121 \times 320 \times 121$ (M2) nodes for the SAILOR code and approximately $4 \cdot 10^6$ cells for simulation using the ANSYS Fluent code. The results of calculations are shown in Fig. 5. Temperature and vertical (V) and horizontal (U) velocity values were compared at selected heights from the inlet. It can be seen that also in this case the compatibility between the results is very good, both the temperature field and the velocities of both simulations are almost identical. It proves that the applied IB-VP method and the solution algorithm are accurate and formulated correctly.

It should be noted that preparing a body-fitted mesh in these relatively simple configurations was not difficult. However, the geometry shown in Fig. 3 required the definition of small, thin cylinders at the point of contact between the spheres. Otherwise, the meshing process caused very distorted cells near the contact points. The applied IB method is free from such problems, i.e. fixed objects can be in any form of contact and even deform each other.

4.2 Heat Transfer in the Single and Double Layer Barriers

The results obtained showed that IB-VP approach could be applied for modelling of the heat and fluid flow in complex domains and around solid objects. In this subsection we analyse the heat transfer inside two industrial configurations of the insulation barriers. They are shown schematically in Fig. 6 along with the locations of the thermocouples used for temperature measurements. The first barrier is composed of single layer granular material (expanded clay, see Fig. 2c), with heat diffusivity equal to $\alpha_g = 8.0 \times 10^{-7} m^2/s$. In the second case there are two-layers composed of granular material and concrete (see Fig. 2b, $\alpha_c = 6.8 \times 10^{-7} m^2/s$). In the experiment the length (L_x), height (L_y) and width (L_z) of the layers were equal to $0.12m$, $0.3m$, $0.3m$, respectively. The layers were insulated from the top and bottom ($y = \pm Ly/2$) and at $z = \pm L_z/2$. In the simulations the dimensions of the barriers were $L_x = 0.12m.$, $L_y = 0.04m$, $L_z = 0.04m$ and at $y = \pm Ly/2$ and at $z = \pm L_z/2$ we assumed adiabatic conditions. Taking smaller layer for the simulations was necessary because of very high computational costs that would be required for the full scale model. For the layer composed of the granulate we assumed the following options: (i) uniform material with an effective heat diffusion coefficient obtained from experiment ($\alpha_g = 5.3 \times 10^{-7} m^2/s$); (ii) spherical ($D = 10mm$) granules with empty spaces filled with air ($\alpha_{\text{air}} = 1.9 \times 10^{-5} m^2/s$); the layer was represented by $13 \times 5 \times 5$ orderly packed spheres. For the latter configuration we considered the cases in which the air was stagnant and when it was flowing from the bottom. In this configuration two buffer layers were added to the domain, i.e. $0.02m$ from the bottom and $0.04m$ from the top. They were required to specify the inlet and outlet boundary conditions and to minimise their impact on the flow in between the spheres. In the performed simulations the mesh was uniform and consisted of $256 \times 208 \times 84$ nodes. The preliminary tests have shown that such a mesh is dense enough to obtain qualitatively consistent solutions.

Initially, the temperature of the barriers was uniform and equal to $298K$. Then, on the right hand side that was treated as an external building side (see Fig. 6), the temperature started to decrease such that at the time $16100s$ it has fallen down to $265K$, we assumed the linear decrease according to $T(t) = 298 - 2.083 \times 10^{-3} t[K]$. The changes of temperature inside the layers were computed by IB-VP approach and were measured by thermocouples

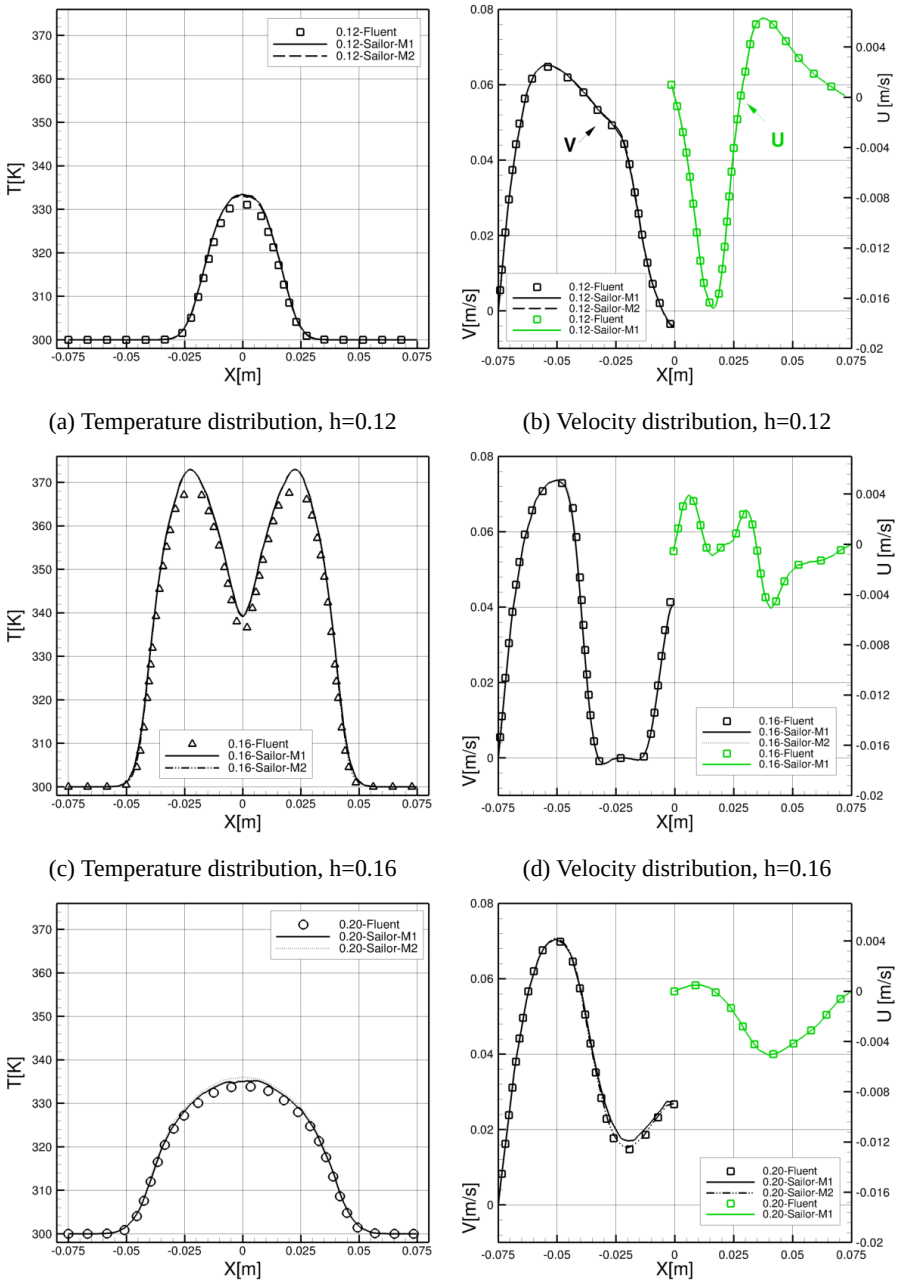

(a) Temperature distribution, h=0.12

(b) Velocity distribution, h=0.12

(c) Temperature distribution, h=0.16

(d) Velocity distribution, h=0.16

(e) Temperature distribution, h=0.20

(f) Velocity distribution, h=0.20

Figure 5: Temperature and velocity profiles in the flow around heated spheres

for additional verification of the applied IB-VP method. In the following part we first compare which configuration is more effective from the point of view of insulation and next we verify whether the assumption of the granular layer as the uniform material with the effective heat diffusivity is accurate. Then, we analyse what happens inside the layers when the air in between the granules starts to move. Note, that such an internal flow can be caused by the natural convection or can be enforced by external sources, e.g. by air-condition system which removes air from buildings and pumps it outside.

Figures 7 present a comparison of numerical results with experimental data for the single-layer and two-layer barriers, respectively. The results obtained from the SAILOR code were verified by experimental data and simulation results achieved using the ANSYS Fluent package. It should be noted that the values obtained by IB-VP method and the ANSYS Fluent are convergent. A slight difference between the results of numerical calculations and experimental data can be attributed to the complex structure of the granular bed and problems with accurate placement of thermocouples and thus with precise data reading. This may have caused deviations from the numerically obtained temperature distribution. Additionally, Fig. 7(on the left side, single-layer barrier) presents data from the barrier,

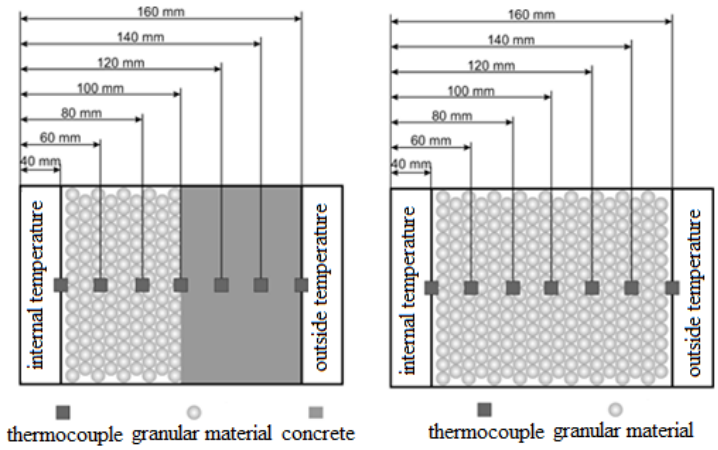

Figure 6: Wall barriers with a schematic distribution of thermocouples

which includes air-filled inter-granular spaces (dashed line denoted as GR+AIR). Differences in the temperature represented by solid lines (uniform material with effective conductivity) are large and originate from the fact that inter-granular spaces filled with air have larger thermal conductivity. This leads to faster temperature change in the entire layer, it is seen that at the end of the layer at the position $x = 0.04m$ at the time $12000s$ the temperature is approximately $10K$ lower compared to the case with effective conductivity. It seems that in this particular case modelling of the heat flow trough the layer assuming an overall heat conductivity is more accurate than treating the layer with different heat conductivities of the solid and air. It can be caused by incorrect specification of the solid material properties provided by the producer.

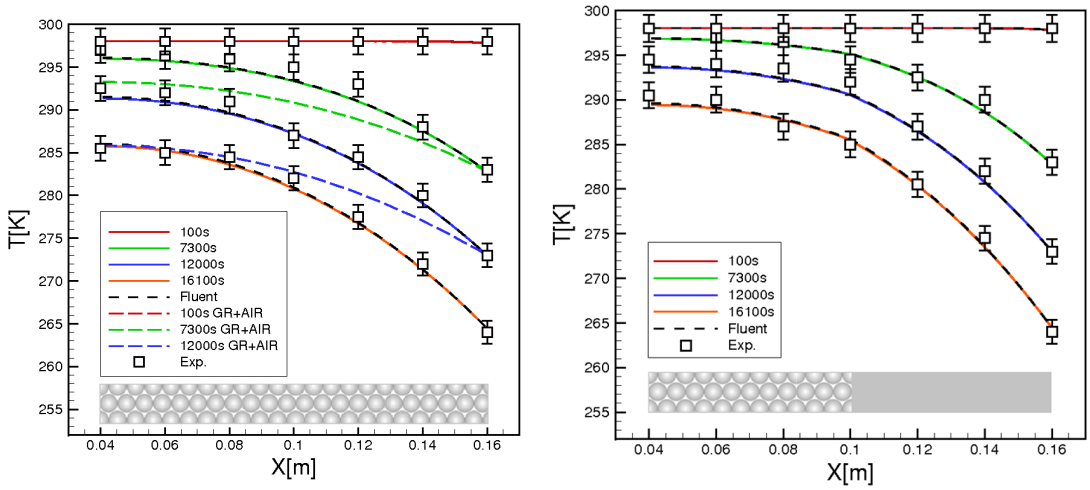

Figure 7: Comparison of numerical results with experimental data: On the left: for a single-layer barrier. On the right: for a two-layer barrier

The results for the two-layer barrier are shown at Fig. 7(on the right side). As in the previous case the differences between numerical and experimental data are small. One can notice that in this configuration the decreasing temperature propagates slower due to smaller heat diffusivity of the concrete. It is worth paying attention to the shape of temperature profiles at the point $x = 0.1m$. This is the point of connected layers of different structure. One can notice a slight inflection, which indicates that the shape of the profiles changes at this point. This test case was used only for validation purpose without involment of the IB method.

4.3 Simultaneous Heat and Flow Fluid in Single Layer Barrier

Next we focus on the case in which the air flows through the barrier. We consider the configuration presented at Fig. 7(on the left side, single-layer barrier) and as the initial solution we take the results at the time instant $12000s$. The air with the temperature $300K$ flows from the bottom side of the barrier with a uniform velocity equal to

$0.1m/s$. Figure 8 shows the temperature and velocity iso-surfaces and velocity vectors for the time 4 seconds from the beginning of the simulation.

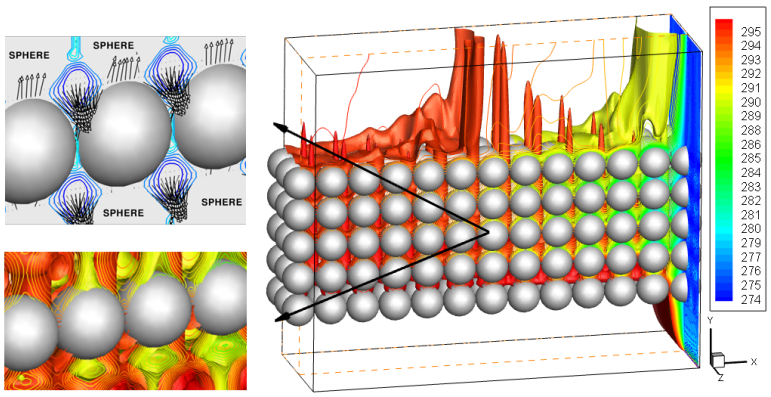

Figure 8: Isosurfaces of temperature and velocity and velocity vectors in the granular bed

The air entering the system is hotter then the barrier temperature and this implies that the temperature distribution should change. Observing the distribution of velocity vectors one can notice local regions of recirculation with locally downward flow. In the direction parallel to the direction of the air inlet one can see clear traces of the low temperature behind the balls. Visibly higher flow temperatures can be observed between granules in inter-granular spaces as evidenced by red iso-surfaces. The red peaks indicate a rapid flow of air. Such an inhomogeneity of flow occurring around individual spheres intensify the heat exchange process. Figure 9 on the right side shows the flow velocity distribution between the spheres and passing through them. It is worth paying attention to the zeroing of the flow velocity in the cross-section, where these regions are marked with white color, and to the places where the local velocity significantly exceeds the inlet velocity (color). This is because in the area of the granular material the spheres occupy most of the volume and the flow must accelerate for the reason of mass conservation. On the contrary, in the plane passing through the spheres (Fig. 9 on the left side) significantly lower velocity values are observed and the spaces between the spheres characterize mostly negative velocity.

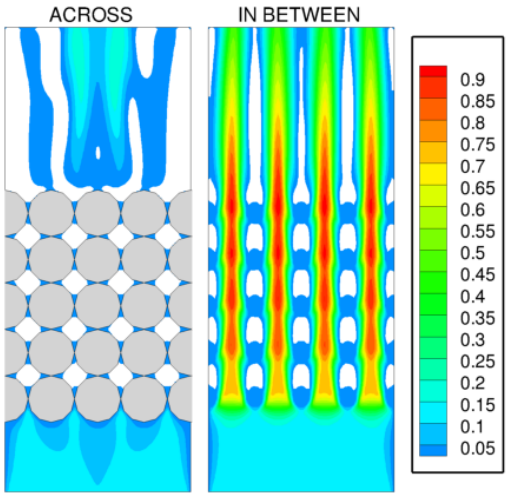

Figure 9: On the left: velocity in the plane passing through the spheres. On the right: velocity in the plane between the spheres.

Figure 10 shows the temperature distribution in the main cross-section ($z = 0$) at the selected time instances. It is seen that it significantly changes across the layer, both along the vertical/horizontal coordinate and between the regions of particular spheres. Compared to the inter-granular spaces they remain colder for long time. Figure 11 show the profiles of temperatures extracted from data presented in Fig. 10 for the time instances $0.1s$, $1s$, $2s$ and $4s$ from the beginning of the simulation. The temperature variations across the layer are shown in two different vertical locations and at four time instances. The dashed line shows the distribution from the location $y = 0.04m$ and the continuous lines correspond to the location $y = 0.06m$. The wavy shape of the profiles reflects varying thermal properties of the granules and air. This shape is readily apparent and becomes more noticeable with time as the cold air from the places in beetwen spheres slowly mixes with the flowing hot air. In the same time the spheres

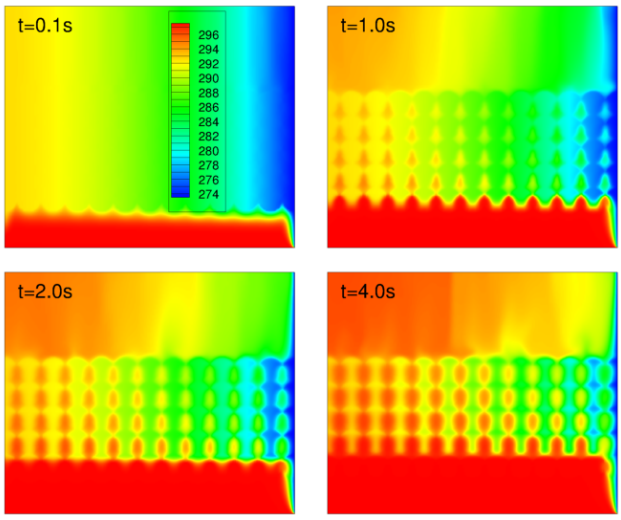

Figure 10: Temperatures in the plane passing through the spheres

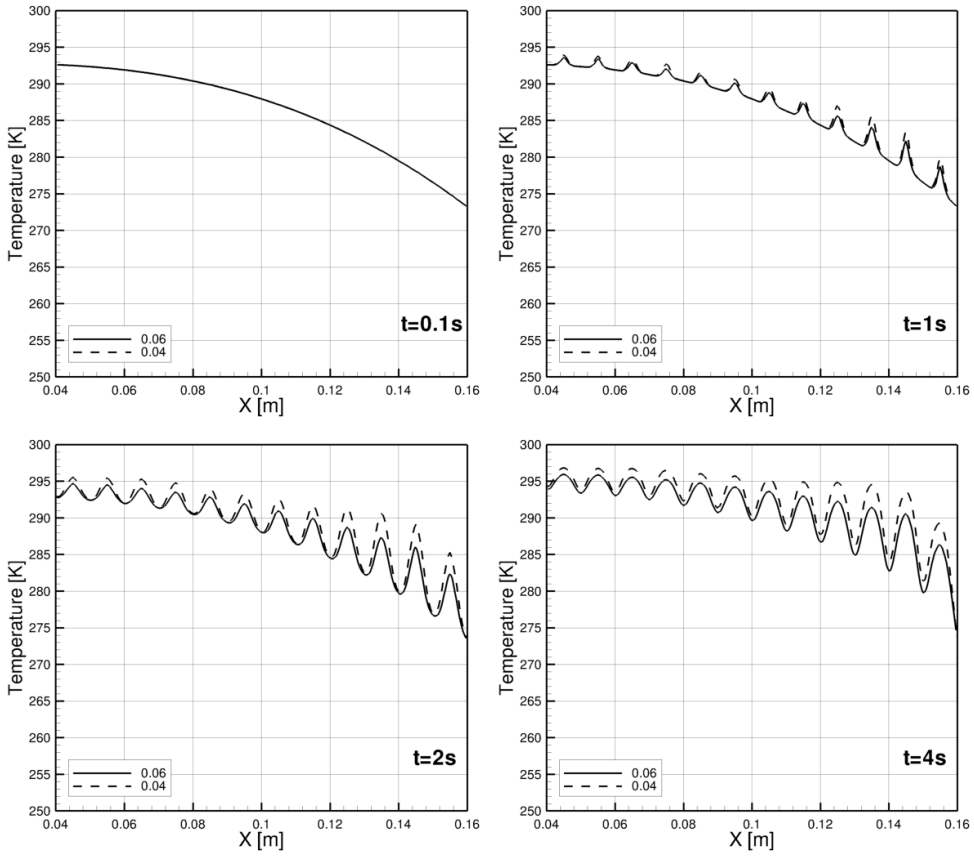

Figure 11: Temperature distribution in the granular bed at four time steps: t = 0.1s, 1.0s, 2.0s and 4.0s in the locations y=0.04m and y=0.06m.

remain cold and get hotter only after while, as it was mentioned above. Although the presented solutions have strongly unsteady character it should be mentioned that for long simulation time the temperature of the flowing air will rise and equalise the temperature of the sphere.

5 Summary

The paper presented numerical and experimental studies on the heat and flow in granular material and external barriers composed of two kind of materials. Comparisons of the numerical and experimental data indicated satisfactory agreement, both for basic test cases as well as for the granular layers and concrete layer used in the barriers. It was shown that treatment of the granulates as uniform layers with effective thermal properties leads to different results than in the case when the granular layer is considered as a complex system of solid material and inter-granular spaces. It was shown that the temperature inside the barriers can be effectively controlled by the motion of air inside the granular layer. In this case the flow and temperature distributions revealed large spatial inhomogeneities where correct predictions are possible only with the help of advanced numerical tools. It is believed that IB-VP method presented and used in this paper is one of them.

Acknowledgements

This work was supported by National Science Centre, Poland (Grant no. 2017/27/N/ST8/02318) and statutory funds of Czestochowa University of Technology under BS/MN 1-103-301/2018/P. PL-Grid infrastructure was used to carry out the computations.

References

[1] lvarez de Miguela, S., Gonzalez-Aguilara, J., Romero, M.; 100-Wh multi-purpose particle reactor for thermochemical heat storage in concentrating solar power plants, *Energy Procedia*, 49, (2014), 676 683.

[2] Yancy-Caballeroa, D.M., Biegler, L.T., Guirardello, R.; Large-scale DAE-constrained optimization applied to a modified spouted bed reactor for ethylene production from methane, *Computers and Chemical Engineering*, 113, (2018), 162183.

[3] Baumann, T., Zunft, S.; Properties of granular materials as heat transfer and storage medium in CSP application, *Solar Energy Materials and Solar Cells*, 143, (2015), 3847.

[4] Ma, Z., Glatzmaier, G.C., Mehos, M; Development of solid particle thermal energy storage for concentrating solar power plants that use fluidized bed technology, *Energy Procedia*, 49, (2014), 898 907.

[5] Ratuszny, P.; Thermal energy storage in granular deposits, *E3S Web of Conferences 19*, EEMS 2017, 01022, (2017)

[6] Hoffmanna, T., Riecka, C., Bcka, A., Peglow, M., Tsotsasa, E.; Influence of granule porosity during fluidized bed spray granulation, The 7th World Congress on Particle Technology (WCPT7), *Procedia Engineering* 102, (2015), 458 467

[7] Diez, E., Meyer, K., Bckc, A., Tsotsas, E., Heinricha, S.; Influence of process conditions on the product properties in a continuous fluidized bed spray granulation process, *Chemical Engineering Research and Design*, 139, (2018), 104115.

[8] Szymanek, E.; Blaszczyk, T.; Hall, M.R.; Dehdezi, P.K.; Leszczynski, J.: Modelling and analysis of heat transfer trough 1D complex granular system, *Granular Matter*, 16(5), (2014), 687-694.

[9] Hainsworth, J.M.; Aylmore, L.A.G.: The use of computer assisted tomography to determine spatial distribution of soil water content, *Australian Journal of Soil Research*, 21(4), (1983), 435-443.

[10] Breugem, W.P.; van Dijk, V.; Delfos, R.: Flows Through Real Porous Media: X-Ray Computed Tomography, Experiments, and Numerical Simulations, *Journal of Fluids Engineering*, 136(4), (2014), 040902.

[11] Amhalhel, G.A.; Furmanski, P.: Problems of modeling flow and heat transfer in porous media, *Biuletyn Instytutu Techniki Cieplnej Politechniki Warszawskiej*, 85, (1997).

[12] Massoudi, M.: On the heat flux vector for flowing granular materials - part I,II, *Mathematical Methods in the Applied Sciences*, 29(13), (2006), 1585-1598, 1599-1613.

[13] Vargas, W.L.; McCarthy, J.J.: Heat Conduction in Granular Materials, *AIChE Journal*, 47, (2001), 1052-1059.

[14] Ferrez, J.A.; Liebling, T.M.: Parallel DEM Simulations of Granular Materials, *High Performance Computing and Networking*, Springer Verlag,(2001).

[15] Tian, K.S.; Shu, H.J.: *Progress in porous media research*, Nova Science Publishers, Inc., New York, (2009).

[16] Ordonez-Miranda, J.; Alvarado-Gil, J.J.: Thermal characterization of granular materials using a thermal-wave resonant cavity under the dual-phase lag model of heat conduction, *Granular Matter*, 12, (2010), 569-577.

[17] Fornberg, B.; Steady viscous flow past a sphere at high Reynolds numbers, *Journal of Fluid Mechanics*, 190, (1988), 471.

[18] Dixon, A.G., Taskin, M.E., Nijemeisland, M., Stitt, E.H.; Systematic mesh development for 3D CFD simulation of fixed beds: single sphere study, *Computers and Chemical Engineering*., 35, (2011), 11711185.

[19] Li,S., Yang, J., Wang, Q.; Large eddy simulation of flow and heat transfer past two side-by-side Spheres, *Applied Thermal Engineering*, 121, (2017), 810819.

[20] Qi,Z., Kuang,S., Rong,L., Yu,A.; Lattice Boltzmann investigation of the wake effect on the interaction between particle and power-law fluid flow, *Powder Technology*, 326, (2018), 208221.

[21] Fadlun, E.A.; Verzicco, R.; Orlandi, P.; Mohd-Yusof, J.: Combined Immersed-Boundary Finite-Difference Methods for Three-Dimensional Complex Flow Simulations, *Journal of Computational Physics*, 161, (2000), 35-60.

[22] Mittal, R.; Iaccarino, G.: Immersed boundary methods, *Annual Review of Fluid Mechanics*, 37, (2005), 239-261.

[23] Khadra, K.; Angot, P.; Parneix, S.: Fictitious domain approach for numerical modelling of Navier-Stokes equations, Caltagirone J-P., *International Journal for Numerical Methods in Fluids*, 34, (2000), 651-684.

[24] Tyliszczak, A.: High-order compact difference algorithm on half-staggered meshes for low Mach number flows, *Computer and Fluids*, 127, (2016), 131-145.

[25] Fletcher, C.A.J.: *Computational Techniques for Fluid Dynamics*, Springer-Verlag, (1991).

[26] Tyliszczak, A.: A high-order compact difference algorithm for half-staggered grids for laminar and turbulent incompressible flows, *Journal of Computer Physics*, 276, (2014), 438-467.

[27] Kadoch, B.; Kolomenskiy, D.; Angot, P.; Schneider, K.: A volume penalization method for incompressible flows and scalar advection diffusion with moving obstacles, *Journal of Computer Physics*, 231, (2012), 4365-4383.

[28] Suekane, T.; Yokouchi, Y.; Hirai, S.: Inertial flow structures in a simple-packed bed of spheres, *AIChE J.*, 49, (2003), 10-17.

Address: Faculty of Mechanical Engineering and Computer Science, Czestochowa University of Technology.
Al. Armii Krajowej 21, 42-201 Czestochowa, Poland
email: ewaszym@imc.pcz.pl email: atyl@imc.pcz.pl